Single-sided NMR to estimate morphological parameters of the trabecular bone structure

Single-sided NMR to estimate morphological parameters of the trabecular bone structure

Marco Barbieri[1,2], Paola Fantazzini[1], Villiam Bortolotti[3], Fabio Baruffaldi[4], Anna Festa[4], David N. Manners[5], Claudia Testa[1,6], Leonardo Brizi[1,6]

[1] University of Bologna, Physics and Astronomy Department, Viale Berti Pichat 6/2 40127, BO, Italy
[2] Stanford University, Department of Radiology, 1201 Welch Rd, Stanford, 94305, CA, USA
[3] Department of Civil, Chemical, Environmental, and Materials Engineering, University of Bologna, Italy
[4] IRCCS Istituto Ortopedico Rizzoli, Via di Barbiano 1/10, 40136 Bologna, Italy
[5] Department of Biomedical and Neuromotor Sciences, University of Bologna, Italy
[6] INFN Bologna, Bologna, Italy.

Corresponding author: Leonardo Brizi, e-mail: leonardo.brizi2@unibo.it

Purpose: Single-sided ^{1}H-NMR is proposed for the estimation of morphological parameters of trabecular bone, and potentially the detection of pathophysiological alterations of bone structure. In this study, a new methodology was used to estimate such parameters without using an external reference signal, and to study intra- and inter-trabecular porosities, with a view to eventually scanning patients.
Methods: Animal trabecular bone samples were analyzed by a single-sided device. CPMG of ^{1}H nuclei of fluids, including marrow, confined inside the bone, were analyzed by quasi-continuous T_2 distributions, and separated into two ^{1}H pools: short and long T_2 components. NMR parameters were estimated using models of trabecular bone structure, and compared with the corresponding micro-CT.
Results: Without any further assumptions, the internal reference parameter (short T_2 signal intensity fraction) enabled prediction of the micro-CT parameters *BV/TV* (volume of the trabeculae/total sample volume) and *BS/TV* (external surface of the trabeculae/total sample volume) with linear correlation coefficient >0.80. The assignment of the two pools to intra- and inter-trabecular components yielded an estimate of average trabecular porosity (33±5)%. Via the proposed models, the NMR-estimated *BV/TV* and *BS/TV* were found to be linearly related to the corresponding micro-CT values with high correlation (>0.90 for *BV/TV;* >0.80 for *BS/TV*) and agreement coefficients.
Conclusion: Low-field, low-cost portable devices, that rely on intrinsic magnetic field gradients and do not use ionizing radiation, are viable tools for *in-vitro* pre-clinical studies of pathophysiological structural alterations of trabecular bone.

Key words: single-sided portable NMR; trabecular bone; morphological parameters; intra-trabecular porosity; bone quality.

1 Introduction

High field whole body MRI is an essential tool for medical diagnosis. It is non-invasive and does not use ionizing radiation. However, low field single-sided NMR [1,2] may also provide an appealing approach for the assessment of biological tissue properties. Single-sided devices have demonstrated their potential in human and animal models like human skin [3,4], silicone breast implants [5], breast tissue [6,7], intestine [8,9], tendon [10], articular cartilage [11], bone [12,13], fluid components of trabecular bone [13], and human mummies [14].

Single-sided devices allow the detection of signal from a sensitive volume (a slab), suitably selected inside an object, regardless of its extension, placed on the magnet surface. They have the additional advantages of low acquisition, running and maintenance costs, as they consist of small permanent magnets, and are portable.

Recently [12,13], we proposed a method for applying single-sided NMR devices to animal trabecular samples, for the evaluation of a parameter commonly used to assess trabecular bone structure, the ratio (*BV/TV*) of the volume occupied by the trabeculae (*BV*) in a sample to the total volume of the sample (*TV*), sometimes referred to as the bone volume fraction.

The development of single-sided NMR strategies for trabecular bone analysis are motivated by the fact that trabecular bone fracture resistance depends not only on bone mineral density (BMD) but also on the trabecular structure [15,16], and that diseases associated with an increase of bone fragility and risk of fractures, such as osteoporosis, have a high impact on human health, quality of life [16,30,31], and health care costs. The clinical standard for the diagnosis of osteoporosis, dual energy X-ray absorptiometry (DXA), employs ionizing radiation, and provides a measure only of the areal BMD [16,17]. Laboratory studies employing NMR, which does not use ionizing radiation, have assessed the structural properties of trabecular bone using relaxometry, diffusometry and magic angle spinning [12,13,18-29]. Clinical MRI assesses bone structure *in vivo* [22,23], but high costs limit its suitability for routine screening. Screening campaigns of the population at risk are desirable, and the development of techniques based on NMR single-sided devices, which could easily be applied at low cost without ionizing radiation, might constitute a future long-term goal.

The procedure proposed in Ref. 12 was based on the computation of the ratio of the ^{1}H nuclei signal from a slab inside the trabecular bone, properly selected using the device, to that from the same slab selected inside an external reference sample, made of bulk marrow. There, the

experimental setup was optimized to acquire the signal at the maximum depth allowed by the device, leading to a low signal-to-noise ratio (SNR) and loss of detail on the short T_2 side of the T_2 distribution of the samples.

In the current work, four spacers between the magnet surface and surface coil were used to maximize the SNR. This permitted the use of an internal reference correlated both to *BV/TV* and to a second parameter, the so called bone surface density *BS/TV* (the ratio of the external surface of the trabeculae in a sample to the total volume of the sample).

We have also investigated the possibility of using NMR to study trabecular bone porosity at different scales. Recent studies have underlined the importance of porosity in both cortical and trabecular bone [32-34]. Ref.s [18,19] introduced the parameter φ_{tb}, the average "intra-trabecular porosity", defined as the volume within the trabeculae not occupied by the mineralized collagen matrix, divided by the total volume of the trabeculae, not including the spaces between trabeculae. That parameter was determined by the analysis of T_1 in defatted and water-saturated samples of animal trabecular bone. In the present work, the definition of φ_{tb} has been adapted to the analysis of T_2 distributions of untreated trabecular samples. We discuss below the level of accuracy with which the parameter φ_{tb} can measure the "intra-trabecular porosity", here defined as the ratio of the volume of the spaces inside the trabeculae occupied by fluids to the total volume of the trabeculae. Simple models are then proposed to formulate NMR estimators of *BV/TV* and *BS/TV*.

Briefly, we have improved the procedure presented in [12] by (i) changing the configuration of the single-sided device, (ii) giving a physical interpretation to the T_2 quasi-continuous distributions, and (iii) applying simple theoretical models to connect NMR data to morphological parameters. The estimated morphological parameters from NMR were validated by comparison with the corresponding micro-CT parameters, which were taken as ground-truth.

2 Methods

Trabecular bone samples

Eleven cylindrical trabecular bone samples, ~1 cm in diameter, ~ 1.5 cm in height, were cored from different sites of pig shoulders, placed inside glass tubes and immediately deep frozen. Bone segments were obtained from the food supply chain; no animals were sacrificed for the purposes of this work. All NMR measurements were performed before micro-CT analysis since preliminary tests demonstrated a loss of the liquid component during the micro-CT measurements.

NMR and micro-CT measurements

Table 1 summarizes instrument information and acquisition parameters for NMR and micro-CT measurements.

*** Table 1 appears near here ***

The following morphological parameters were estimated by micro-CT, after a global image thresholding performed using Otsu's method [35]: the bone volume fraction (*BV/TV* (%)), the bone surface density (*BS/TV* (mm^{-1})), the trabecular number (*Tb.Nb* (mm^{-1})), the trabecular thickness (*Tb.Th*(mm)), the bone surface to bone volume ratio (*BS/BV* (mm^{-1})) and the trabecular pattern factor (*Tb.Pf* (mm^{-1})) that evaluates the connectedness of bone structures.

Figure S1 shows the NMR-MOUSE PM10 (simply MOUSE in the following text) configuration used, with 4 spacers between magnet and coil to maximize the SNR. In [12], the configuration with no spacers was adopted, and only the signal with the longest T_2s could be detected. Sensitivity increased with the number of spacers, at the cost of a reduced penetration depth. In the current configuration, the sensitive volume was located at 3 mm above the surface coil. With the current choice of measurement parameters (Table 1), the theoretical excited slab thickness was 330 μm, rounded to 300 μm taking into account the sinc-shaped frequency distribution.

Trabecular bone tissue can be highly heterogeneous across a sample. Therefore, all samples were marked at one end, and two sensitive volumes were acquired for each sample, by flipping the sample with respect to the coil, obtaining two configurations (*Marker and No-Marker* configurations; Figure S1). We assumed, based on previous experience, that even samples from the same specimens represented structurally different portions of the bone, so that the 22 measurements obtained could be considered independent.

To avoid possible systematic errors we followed this protocol: (1) the sample was left to defrost for 45 minutes; (2) NMR measurement was performed in one of the two configurations; (3) the sample was returned to the freezer; (4) later, acquisition was performed on the remaining configuration.

The morphological parameters were evaluated by micro-CT in the two regions of interest (ROIs) of the sample, trying to match, as best as possible, the regions sampled by the sensitive volume. Such matching was possible due to the presence of the marker and a knowledge of the position and the thickness of the sensitive volume. Figure 1A presents a coronal view of a micro-CT scan of a sample along with examples of axial images of the analyzed ROIs in homogeneous regions of samples (Figure 1B, C) and in 6 samples characterized by tissue heterogeneity (Figure 1 from (D) to (I))

*** Figure 1 appears near here ***

Figure S2 displays image analysis for three bone samples representing three different conditions found in our samples set. Errors associated with the micro-CT measurements were evaluated considering that the main source of uncertainty was the selection of the threshold value for bone segmentation. Hence, morphological parameters were evaluated using different threshold values in the range defined by the "optimal threshold value" estimated by the Otsu's method ± 5%. Examples in Figure S3 show the variation in *BV/TV* estimation for three samples, where the segmentation was performed using 5 different values of the threshold: the "optimal threshold value", and 5 or 10 gray levels above and below this.

^{1}H NMR data were acquired in the time domain using the CPMG pulse sequence and inverted by the algorithm UPEN [36-39], implemented by the software UpenWin [36], to obtain quasi-continuous T_2 distributions. To invert decay data, a regularization parameter that smooths the distributions is normally implemented to reduce excess variation [28,29]. An inversion algorithm using a fixed smoothing coefficient may introduce details into the distribution not required by the data, such as a tail broken into several peaks, even if the coefficient is adaptively chosen based on the noise level of the data. The algorithm UPEN addresses this problem by using a locally variable smoothing coefficient, determined by iterative feedback in such a way that the smoothing penalty is roughly constant along the whole distribution. For comparison, bi-exponential fits were also performed. Figure S4 shows the pipeline used for these two inversion methods.

Background of the proposed procedure

NMR relaxometry studies have found ^{1}H T_2 relaxation times for cortical and trabecular bones that span from hundreds of μs to hundreds of ms [13,18,19,28,29,40,41]. Under our experimental conditions, the signal due to collagen protons, with T_2 10-60 μs, was not detectable. The T_2 quasi-continuous distributions of the remaining fluids are substantially bimodal, with low minima between the two peaks (Figures 2, S4). The marrow will also be considered "fluid", though it contains substances more viscous than bone fluids [42].

The methodology relies on a few assumptions. The first concerns the assignment of the two peaks to two fluid compartments, not connected at the relaxation time scale. Let S_{shortT_2} be the short T_2 and S_{longT_2} the long T_2 peak signal intensities. The total signal intensity will be $S_{total} = S_{shortT_2} + S_{longT_2}$. Let η, the "short T_2 intensity fraction", be the ratio of S_{shortT_2} to S_{total}:

$$\eta = \text{short } T_2 \text{ intensity fraction} = \frac{S_{\text{short } T_2}}{S_{\text{total}}} \qquad (1).$$

A further assumption concerns the relationship between signal intensity and compartment density. The signal is proportional to the amount of ^{1}H due to fluids in each compartment; if the proton densities of the fluids are approximately the same [25], as well as the densities of water and marrow [26], the signals should be proportional to the volumes of the spaces confining the fluids themselves. Further assumptions concern the separation of the two ^{1}H pools and their assignment to intra- and inter-trabecular signals. We set the threshold time at 1 ms to separate the two compartments on the T_2 quasi-continuous distributions (Figure 2A), and as discussed in greater detail below, the short and long T_2 components were assigned to the intra- and the inter-trabecular fluids, respectively.

Following ref. [18, 19], the ratio η can be interpreted as the ratio of the volumes occupied by fluids inside the trabeculae ($V_{\text{intra-tb}}$) to the volume occupied by all fluids in the bone ($V_{\text{tot-fluids}}$), including the spaces between trabeculae:

$$\eta = V_{\text{intra-tb}}/V_{\text{tot-fluids}}.$$

The ratio η should provide a parameter to estimate the intra-trabecular porosity (φ_{tb}), the volume within the trabeculae occupied by the fluids divided by the total trabecular volume. In fact, by knowing the total porosity of the bone (φ_{tot}), defined as the volume occupied by fluids within a

given trabecular bone sample divided by the volume of that sample, the value of φ_{tb} can be computed by Eq. 2 [19]:

$$\varphi_{tb} = \eta\, \varphi_{tot} / (1 - \varphi_{tot} + \eta\, \varphi_{tot}) \quad (2).$$

In a set of animal trabecular bones, the value of φ_{tb} was found to be almost constant, with average value = (29 ± 4) %, for samples having φ_{tot} spanning the range 40-70% [19].

BV/TV estimation from η

The volume occupied by the trabecula can be divided into two main contributions, the volume of the intra-trabecular fluids and that of the mineralized tissue: $BV = V_{tb} = V_{intra\text{-}tb} + V_{mineral}$. The total volume of the sample is $TV = V_{tot} = V_{inter\text{-}tb} + V_{tb}$. By adopting the assumptions discussed above, the volume of the fluids inside the trabeculae is proportional to the intra-trabecular signal $S_{short T2}$, and the volume in the inter-trabecular space ($V_{inter\text{-}tb}$) is proportional to the inter-trabecular signal $S_{long T2}$, while the volume of the mineralized trabecular tissue ($V_{mineral}$) is related the porosity of the trabeculae. For each sample:

$$\varphi_{tb} = \frac{V_{\mathrm{intra-tb}}}{V_{\mathrm{intra-tb}} + V_{\mathrm{mineral}}} \quad (3)$$

implying the *BV/TV* ratio in percent can be expressed, in terms of volumes, by Eq. 4:

$$BV/TV = \frac{\frac{V_{\mathrm{intra-tb}}}{\varphi_{tb}}}{V_{\mathrm{inter-tb}} + \frac{V_{\mathrm{intra-tb}}}{\varphi_{tb}}} \cdot 100(\%) \quad (4),$$

which in terms of NMR signals can be rewritten in Eq. 5:

$$BV/TV = \frac{\frac{S_{shortT_2}}{\varphi_{tb}}}{S_{longT_2} + \frac{S_{shortT_2}}{\varphi_{tb}}} \cdot 100(\%) \quad (5).$$

BS/TV estimation from η

The *BS/TV* ratio can be estimated by modelling the trabeculae as cylinders of radius *R* and height *h*:

$$BS/TV = \frac{2 \cdot \frac{V_{\text{intra-tb}}}{\varphi_{tb}}}{R} \cdot \frac{1}{V_{\text{inter-tb}} + \frac{V_{\text{intra-tb}}}{\varphi_{tb}}} \cdot 100(\%) \quad (6).$$

The first multiplicative factor on the right side of the equation is the expression of the bone surface, which comes from $V_{\text{tb}} = \pi R^2 h$. Since the signal intensities of the long and short T_2 components are proportional to the volumes of the spaces occupied by the inter- and the intra-trabecular fluids, respectively, the *BS/TV* ratio can be written in terms of NMR signals, as expressed in Eq. 7.

$$BS/TV = \frac{2 \cdot \frac{S_{shortT_2}}{\varphi_{tb}}}{R} \cdot \frac{1}{S_{longT_2} + \frac{S_{shortT_2}}{\varphi_{tb}}} \cdot 100(\%) \qquad (7).$$

In each bone sample, R can be considered as the average value of the radius of all the trabeculae. Following Eq. 5. and Eq. 7, the NMR estimates of *BV/TV* and *BS/TV* were computed using estimated values of φ_{tb} and R. Pearson's and Lin's coefficients were used to assess correlation and agreement between NMR and micro-CT parameters.

Errors in the estimates of BV/TV and BS/TV by MOUSE

Mean and standard deviation were computed on thirty repeated measurements of S_{total} performed on a sample made of rubber, not subjected to degradation, tailored to obtain the same SNR level as the bone samples.

The percentage error associated to S_{total} was estimated using the relative standard deviation (RSD) calculated according to Eq. 8:

$$\text{RSD} = \frac{S}{\overline{x}} \times 100 \qquad (8).$$

where S is the standard deviation of the repeated measurements of S_{total}, and $\overline{x}$ is the value of the corresponding average.

The error was found to be ≈1% as was the error associated with the short component. Errors on *BV/TV* and *BS/TV* were then computed using error propagation.

3 Results

Micro-CT analysis

Calculated morphological micro-CT parameters are reported in Table 2. The data demonstrate the variability of bone microstructure both among and within samples. For instance, *BV/TV* ratios ranged from 24% to 53%, with no apparent intrasample correlation. M1-1 is typical: 38% at the bottom and 28% at the top (Figure 1B and 1C, respectively).

Samples M2-2 No Marker and M2-4 Marker, Figure 1G and Figure 1I, were characterized by the highest tissue heterogeneity and have negative *Tb.Pf* in Table 2. A Principal Component Analysis applied to micro-CT parameters (Figure S5) confirmed that these two samples did not belong to the same set and were therefore excluded from the comparison between NMR and micro-CT results.

*** Table 2 appears near here ***

NMR results

CPMG data analysis and separation between intra- and inter-trabecular signals

Figure 2 shows the quasi-continuous and bi-exponential T_2 distributions of the samples. The quasi-continuous distributions (Figure 2A) were substantially bimodal, ranging from around 0.1 up to hundreds of ms, including a trough from 1 to 10 ms. The bi-exponential fit in Figure 2B displayed a sharp separation between shorter and longer T_2 components, with a short T_2 component less than 1 ms in all samples. Residual analysis performed on the fits of each method showed that fitting errors were comparable; fit mean percentage error (MPE) was (-0.04 ± 0.03) % and (-0.06 ± 0.02) % for quasi-continuous and bi-exponential fits, respectively, while corresponding root mean squared errors (RMSE) were 0.014 ± 0.001 and 0.016 ± 0.001.

As our later results will show, even though fit errors of both models are comparable, the bi-exponential approach does not accurately model the structure of the trabecular bone.

*** Figure 2 appears near here ***

Analysis of trabecular bone structure by T_2 quasi-continuous distributions

Assessing correlations between η and micro-CT morphological parameters

Figure 3 displays the results of an experiment in which samples of trabecular bone, cortical bone and marrow were analyzed in homogeneous and inhomogeneous magnetic fields. A comparison of the results justifies the use of a threshold at 1 ms to separate intra- and inter-trabecular signals. Further discussion of this point is postponed until Discussion and Conclusions.

Figure 4 (A, B, C) shows a significant linear regression of η, computed using the 1 ms threshold, against the micro-CT parameters *BV/TV*, *BS/TV*, and *Tb.Nb*. In each case, the correlation coefficient is $r > 0.80$.

*** Figure 3 appears near here ***

*** Figure 4 appears near here ***

Analysis of the intra-trabecular porosity

The mean intra-trabecular porosity (φ_{tb}) of a trabecular bone sample can be estimated from its T_2 distribution by Eq. 2, knowing its total porosity (φ_{tot}). For each sample, an estimate of the φ_{tot} was found by dividing the signal of the sensitive volume detected by the MOUSE inside the bone sample by the signal from the same sensitive volume acquired on a reference sample, made of bone marrow. The φ_{tb} values of the samples are reported in Table 3, along with the corresponding values of η and φ_{tot}, and compared with the values reported in ref. 19. The difference between the two means was not significant (p=0.12) (Figure S6).

*** Table 3 appears near here ***

The φ_{tb} of each sample was also estimated starting from the bi-exponential analysis of CPMG data, obtaining $(27 \pm 3)\%$, significantly different from the mean value obtained by the quasi-continuous distributions $(33 \pm 5)\%$ (based on a t-test, $p = 2.4 \times 10^{-5}$ - Figure S7).

BV/TV and BS/TV estimations: direct comparison between NMR and micro-CT estimates

*** Figure 5 appears near here ***

Three different procedures were followed to estimate *BV/TV* and *BS/TV* by NMR. The comparison between NMR and micro-CT estimates is summarized in Figure 5. When average φ_{tb} values are available, they can be used to overcome the need for a reference sample. In Figure 5A and 5B**,** the mean value of φ_{tb} available in the literature (29%) [19], and in Figure 5C and 5D the mean value of our samples, φ_{tb} =33% (Table 3), was used. Without recourse to an average, the reference is needed to estimate the individual φ_{tb} for each sample. This approach is demonstrated in Figure 5E and 5F. To estimate *BS/TV* by Eq. 7, an estimated of the mean trabecular radius *R* is also needed. We used half of the mean trabecular thickness computed by micro-CT (Table 2) (Figure 5B, D, F). The correlation coefficients were >0.90 for *BV/TV* and >0.80 for *BS/TV* with very good agreements as shown by the values of the Lin's coefficients.

Bland-Altman (B-A) plots for the comparison of NMR and micro-CT estimates of morphological parameters *BV/TV* and *BS/TV* are presented in Figure 6. They show that the estimates of *BV/TV* and *BS/TV* obtained by the two methods are equivalent when the sample-specific φ_{tb} is considered. The use of fixed φ_{tb} = 29% resulted in the highest mean bias, most significantly different from zero.

*** Figure 6 appears near here ***

The comparison between NMR and micro-CT *BV/TV* and *BS/TV* estimates computed by bi-exponential analysis showed strong correlations but only weak to moderate agreement, as highlighted by the bias terms of the linear fits (Figure S8).

BV/TV and BS/TV estimations: minimization of the mean squared error (MSE) between NMR and micro-CT estimates

To retrospectively find the φ_{tb} and trabecular radius required in Eq. 5 and 7 to minimize the mean squared error (MSE) between NMR and micro-CT estimates of *BV/TV* and *BS/TV*, different values of φ_{tb} and trabecular radii were tried and MSE computed for each trial (Figure 7A and B). The optimal φ_{tb} was found to be 35%, while *R* was 90 μm. Figures 7C and D show the corresponding correlations between NMR and Micro-CT.

*** Figure 7 appears near here ***

The same analysis performed using data obtained by the bi-exponential fits showed, Figure S9**,** that the best value for φ_{tb} was 46%, considerably higher than (33±5)%, and the best trabecular radius was ~ 130 μm, 50% higher than the expected value.

4 Discussion and Conclusions

Our results rely on a few assumptions, the most demanding of which concern the analysis and the interpretation of the T_2 quasi-continuous distributions of trabecular bone, approximated in the present work by bi-modal distributions. These assumptions regard *(i)* the assignment of the two ^{1}H pools to intra- and inter-trabecular components, and *(ii)* the threshold, set at 1ms, to separate signals from the two pools (Figure 2).

Water in bone is present at various locations and in different states [24]. In cortical bone, a small fraction of water exists in a form that can be considered "free" (the so-called *pore water*) in Haversian canals (typical diameters ~50-200 μm), in lacunae (~5 μm) and in canaliculi (~0.1 μm) [43,44]. CT images at high resolution provide information about dimensions, amounts, and locations of these volumes [32-34]. A larger amount of water, the so-called *bound water*, is bound to collagen [28,40,41].

In cortical bones from human samples, three components have been identified by CPMG [28,40,41]: a component with T_2 ~60 μs, from collagen side-chains, a second one with T_2 ~400 μs, the *bound water*, and finally a third component with $T_2 > 1$ ms, ascribed to lipids and to the *pore water*. The bound- and pore-water was also quantified by Ultrashort Echo Time (UTE) in animal cortical samples [44,45]. In Ref. [28], based on micro-CT at 6 μm isotropic resolution, Haversian canal porosity was quantified as (4.0 ± 1.0) %, and a similar porosity was assigned to lacunar-canalicular spaces. Moreover, it was suggested that this latter portion of the pore water might be included in the $T_2 \approx$ 400 μs component [28], and this is consistent with the smaller sizes of such spaces (0.1 – 5 μm), compared to those of the Haversian canals (50-200 μm), whose signal should contribute to the longer T_2 component.

Following Ref. [42] three levels of bone porosity are found within the cortical bone: the vascular porosity, the lacunar–canalicular porosity and the collagen–apatite porosity, all containing fluids. The lacunar–canalicular porosity and the collagen–apatite porosity are also

found within the trabeculae of the trabecular bone. In trabecular bone, there is the further porosity contributed by the inter-trabecular space containing marrow, fat, and blood vessels.

Therefore, we can assume that the signal from the fluids inside the trabeculae is due, in larger amount, to the water bound to collagen (the *bound water*), with a smaller contribution due to the *pore water* of the lacunar-canalicular porosity, and that those fluids generate the short T_2 peak. The signal from the inter-trabecular fluids forms the long T_2 peak, distinct from the short T_2 peak because the two environments are not connected at the relaxation time scale.

Regarding the justification for setting the threshold at 1 ms, the comparison of the T_2 distributions obtained in the homogeneous magnetic field of a home-made relaxometer and in the inhomogeneous field of the MOUSE for animal cortical bone and trabecular bone are shown respectively in Figure 3A and Figure 3B, while the distributions for trabecular bone, cortical bone and a sample of bulk marrow, all obtained by the MOUSE are compared in Figure 3C.

The single-sided device should induce a shift of the water signals to shorter T_2s, due to the molecular diffusion inside its field gradient. In Figure 3A**,** the same tail for $T_2 > 1$ ms is shown for both devices, suggesting that the amount of water in the Haversian canals, if any, was negligible. The broadening of the short T_2 peak (T_2<1ms) shown by the single-sided device is explained by the shift to even shorter times by diffusion of water in the lacunar-canalicular spaces.

The effects of diffusion appeared in both the cortical and the trabecular bone (Figure 3A and 3B). In Figure 3B, the single-sided device shows the shift to shorter times for water signal inside the inter-trabecular spaces, over the range 1-10 ms, while the signal obtained inside a homogeneous magnetic field blends into the baseline. Figure 3C shows that the marrow signal does not contribute to the range from 1 to 2-3 ms, where the signal from trabecular bone is high. Therefore, the signal from fluids in the inter-trabecular space is present in this range. The threshold at 1 ms is a compromise that avoids losing part of the signal of the intra-trabecular water while simultaneously reducing the possible contribution to shorter T_2 of the inter-trabecular water shifted by diffusion to shorter times.

Taken together, these considerations suggested that the parameter η, the short T_2 intensity fraction, could provide an internal reference signal. This parameter showed linear correlations, with high Pearson's coefficient (r> 0.80; p<0.001), with the micro-CT estimates of *BV/TV*, *BS/TV* and *Tb.Th* (Figure 4). Therefore, this newly proposed procedure requires no external reference to predict *BV/TV*, and in addition provides information on *BS/TV* and *Tb.Th*.

The present work also aimed to find methods based on single-sided NMR of estimating the average porosity of the trabeculae, here named the intra-trabecular porosity, (φ_{tb}), the ratio of the volume of the fluids inside the trabeculae to the total volume of the trabeculae. To estimate φ_{tb}, a knowledge of the total porosity φ_{tot} of the sample was needed. This could be determined by weight, or, as shown above, by comparison of the sample signal with that of the reference sample made of marrow. Such a procedure reintroduces the need for an external reference, but, at the same time, it allows φ_{tb} to be estimated for each sample, using η and φ_{tot} in Eq. 2. This method provided the average value of the intra-trabecular porosity of our set of samples (33±5) %, (Table 3).

Regardless of how the value of φ_{tb} is derived (by an external reference, by weight, or from the literature), it is straightforward, through Eq. 5 and 7, to provide robust NMR estimators, expressed in the same units as the micro-CT estimated quantities, of the parameter *BV/TV*, and, through the introduction of the radius parameter, *R*, of *BS/TV*, also. It is worth noting that the correlations and agreements are better than the ones computed by the use of η (Figures 4 and 5).

A new method for investigation of the values of φ_{tb} and *R* is demonstrated here, namely the minimization of the error of the agreement between NMR and micro-CT estimated parameters (Figure 7). This error minimization method can usefully be applied in the laboratory for *in vitro* studies of the structure of different kinds of trabecular bones. Figures 7A and 7C show the results for *BV/TV*. The minimum squared error was obtained by setting φ_{tb} = 35% (Figure 7A), a value within the interval (33±5)% of data measured for the samples of the present study (Table 3, Figure S6). Figure 7B and 7D show the results for *BS/TV*. The minimum squared error was obtained by setting *R* = 90 μm (Figure 7B), close to the expected value, and consistent with half the mean trabecular thickness (Table 2).

In order to investigate different approaches to data modelling, we compared the results obtained by both quasi-continuous and bi-exponential distributions (Figure 2). Both models were able to provide good fits to CPMG data, with comparable errors (Figure S4), but bi-exponential analysis did not adequately estimate the morphological parameters (Figure S7, S8, S9). The bi-exponential analysis has the advantage of fitting the data using a small number of parameters, but even if the two models fit the experimental data equally well, their assumptions differ greatly. As previously noted [29], "it is important to keep in mind that bi-component analysis, whether based on T_2* or T_2, and whether performed in one or two dimensions, involves one major, and incorrect,

assumption: the existence of two pools with discrete relaxation times. T_2 values are instead distributed continuously over several orders of magnitude".

In conclusion, we were able to improve the procedure presented in [12] by *(i)* changing the configuration of the single-sided device (Figure 1, Figure S1), *(ii)* giving a physical interpretation to the T_2 quasi-continuous distributions, and *(iii)* applying simple theoretical models to connect NMR data to morphological parameters.

The novelty is not limited to this improvement since the newly proposed procedure is able to assess trabecular bone structural parameters other than *BV/TV*, such as *BS/TV* and intra- and inter-trabecular porosities.

The literature does not clearly establish the extent to which diseases affecting bone tissue modify its structure at the intra- and inter-trabecular levels, although parameters such as the intra- and inter-trabecular porosities may vary with such diseases. It is not clear whether the imbalanced and excessive bone remodeling that occurs in bone pathologies only affects the trabecular network, by removing some trabeculae, or if it also affects the intra-porosity of the trabeculae themselves. Having established a method to investigate trabecular bone structure with single-sided NMR, even at the intra-trabecular level, future studies can focus on assessing these effects.

The strong level of correlation and agreement between NMR and micro-CT estimators demonstrates that our NMR methodology is adequate for parameterizing trabecular structure, at least as well as micro-CT does. Of course, the method is affected by certain limitations. It relies on models that over-simplify a complex biological system. Intrinsic limitations are the low signal-to-noise ratio, and some physical assumptions. The measured T_2 values are not pure T_2, as they are affected by diffusion; moreover, T_2 distributions are obtained by inversion algorithms that try to solve a problem that is intrinsically ill-posed. The 1 ms threshold, even though justified here by morphological and physical considerations, introduces an element of arbitrariness into signal assignment.

Nevertheless, the results presented give grounds for confidence in the usefulness of single-sided NMR for studying bone porosity at different scale levels, and provide a future way to study the variations of the bone porosities associated with bone diseases. If this confidence is justified, while the proposed methodology is still a long way from possible extension to scanning patients, it is possible to envisage screening campaigns conducted on populations at risk of bone diseases, such as osteoporosis, thanks to the low cost and portability of the device. On the medical-scientific

side, future studies need to assess the effects of bone diseases on trabecular structure. On the technical side, it is necessary to identify the most appropriate region of the body for scanning, possibly easily accessible structures such as calcaneus or distal radius. The hardware (magnet and coil) could then be redesigned to properly fit that region. Even if much work is still needed in those directions, we consider our results to be a significant step towards the long-term goal of the use of single-sided NMR systems for in-vivo applications.

Acknowledgements

The “Centro Fermi - Centro Studi e Museo Storico della Fisica, Enrico Fermi” and the “Fondazione del Monte di Bologna e Ravenna” partially contributed to complete the setup of the NMR-MOUSE PM10, equipped with the lift and the console for automatically data producing and acquisition.

Data availability statement

The data that support the findings of this study are openly available in AMSACTA-UNIBO at http://amsacta.unibo.it/id/eprint/6534.

NMR		Micro-CT	
Instrument	NMR-MOUSE PM10 (*)	Instrument	Skyscan micro-CT mod.1072(**)
Spectrometer	KEA II (*)	X-ray source	50 kV - 200 µA
Acquisition Software	Prospa (*)	Resolution	20 µm (pixel size)
Configuration	4 spacers inserted	Rotation	180 degree - on its axis
Spacer Thickness	2 mm	Rotation step	0.9 degree
Frequency (^{1}H)	13.88 MHz	# of projections	206
Magnetic field gradient	14 T/m	Reconstruction	NRecon software ver. 1.6.8.0 (**)
Pulse length	5 µs	Analysis	CtAnalyser ver. 1.14.4.1 (**)
Pulse Sequence	CPMG	Threshold	Otsu's method
Echo Time (T_E)	50 µs		
Number of Echoes	2000		
Repetition Time	6 s		
Number of Scans	128		
Total acquisition time	~13 minutes		
(*) Magritek Ltd, Wellington, NZ		(**) Bruker MicroCT, Konthich, Belgium	

Table 1. Details and parameters of NMR and Micro-CT measurements

Sample	Orientation	*BV/TV* (%)	*BS/TV* (%)	*Tb.Nb* (mm^{-1})	*BS/BV* (mm^{-1})	*Tb.Th* (mm)	*Tb.Pf* (mm^{-1})
M1-1	No Marker	38	9.1	2.26	23.7	0.171	5.3
M1-1	Marker	28	6.4	1.65	23.0	0.170	6.0
M1-2	No Marker	41	9.2	2.31	22.4	0.178	4.2
M1-2	Marker	36	7.7	1.99	21.6	0.180	3.1
M1-3	No Marker	45	9.9	2.54	22.0	0.177	2.4
M1-3	Marker	31	6.2	1.59	20.6	0.189	5.6
M1-4	No Marker	44	10.7	2.70	23.9	0.166	-4.5
M1-4	Marker	32	7.5	1.92	23.1	0.170	4.3
M1-5	No Marker	35	8.1	2.03	23.7	0.168	-1.4
M1-5	Marker	26	6.1	1.61	23.6	0.160	5.5
M2-1	No Marker	34	9.0	2.23	26.5	0.152	4.7
M2-1	Marker	29	7.6	1.94	25.5	0.154	0.1
M2-2	No Marker	51	13.7	3.62	26.3	0.144	-27.8
M2-2	Marker	33	7.4	1.83	22.9	0.177	6.5
M2-3	No Marker	24	6.7	1.61	27.9	0.148	9.9
M2-3	Marker	38	7.5	1.95	20.0	0.193	2.0
M2-4	No Marker	28	7.0	1.70	25.0	0.164	7.9
M2-4	Marker	53	12.8	3.60	24.9	0.143	-18.8
M3-1	No Marker	44	9.0	2.22	20.3	0.201	1.5
M3-1	Marker	41	8.5	2.16	20.4	0.192	1.5
M3-2	No Marker	45	11.1	2.77	24.7	0.162	0.1
M3-2	Marker	34	8.1	2.16	23.6	0.160	4.3

Table 2. Morphological parameters of the trabecular bone samples estimated using micro-CT.

This study (*)					Ref. [19]		
Sample label	Orientation	η (%)	φ_{tot} (%)	φ_{tb} (%)	Sample label	φ_{tot} (%)	φ_{tb} (%)
M1-1	Marker	14	76	31	1	66	31
M1-1	No Marker	19	73	34	2	56	30
M1-2	Marker	20	77	40	3	55	29
M1-2	No Marker	20	70	32	4	46	31
M1-3	Marker	12	74	25	5	44	30
M1-3	No Marker	23	72	38	6	65	34
M1-4	Marker	13	73	27	7	60	26
M1-4	No Marker	22	76	41	8	48	25
M1-5	Marker	8	76	20	9	54	26
M1-5	No Marker	14	78	34	10	59	26
M2-1	Marker	11	84	37	11	58	25
M2-1	No Marker	14	77	32	12	72	36
M2-2	Marker	16	80	39	13	69	22
M2-3	Marker	18	77	37	14	67	38
M2-3	No Marker	10	79	27	15	63	33
M2-4	No Marker	14	81	37			
M3-1	Marker	20	71	34			
M3-1	No Marker	21	71	34			
M3-2	Marker	15	77	33			
M3-2	No Marker	23	78	32			
				Mean ± Std 33 ± 5			Mean ± Std 29 ± 5

Table 3. Values of η, φ_{tot}, and φ_{tb} for the trabecular bone samples considered in this study and intra-trabecular porosity reported in ref. 19.
(*) Each measurement was affected by an error in the order of a few percentage units. It is worth mentioning that, for this comparison, the four samples in which growth cartilage and less mineralized bone tissue were present were excluded from the test, which are 4 out of 20 samples, because samples with these characteristics were not present in the set of samples used in [19].

References

[1] Blümich B, Blümler P, Eidmann G, Guthausen A, Haken R, Schmitz U, Saito K, Zimmer G. The NMR-mouse: construction, excitation, and applications. Journal of Magnetic Resonance Imaging. 1998;16:479–484.

[2] Blümich B. Low-field and benchtop NMR. Journal of Magnetic Resonance. 2019;306:27-35. doi:10.1016/j.jmr.2019.07.030

[3] Landeghem MV, Danieli E, Perlo J, Blümich B, Casanova F. Low-gradient single-sided NMR sensor for one-shot profiling of human skin. Journal of Magnetic Resonance. 2012;215:74–84.

[4] Bergman E, Sarda Y, Ritz N, Sabo E, Navon G, Bergman R, Nevo U. In vivo assessment of aged human skin with a unilateral NMR scanner. NMR in Biomedicine. 2015;28(6):656–666.

[5] Krüger M, Schwarz A, Blümich B. Investigations of silicone breast implants with the NMR-MOUSE. Journal of Magnetic Resonance Imaging. 2007;25:215–218.

[6] Ali TS, Tourell MC, Hugo HJ, Pyke C, Yang S, Lloyd T, Thompson EW, Momot KI. Transverse relaxation-based assessment of mammographic density and breast tissue composition by single-sided portable NMR. Magnetic Resonance in Medicine. 2019;82(3):1199–1213.

[7] Bashyam A, Frangieh CJ, Li M, Cima MJ. Dehydration assessment via portable, single sided magnetic resonance sensor. Magnetic Resonance in Medicine. 2020;83(4):1390-1404. https://doi.org/10.1002/mrm.28004

[8] Keschenau PR, Klingel H, Reuter S, et al. Evaluation of the NMR-MOUSE as a new method for continuous functional monitoring of the small intestine during different perfusion states in a porcine model. PLoS One. 2018;13(11):e0206697. Published 2018 Nov 2. doi:10.1371/journal.pone.0206697

[9] Keschenau PR, Simons N, Klingel H, et al. Perfusion-related changes in intestinal diffusion detected by NMR-MOUSE® monitoring in minipigs. Microvascular Research. 2019;125:103876. doi:10.1016/j.mvr.2019.04.006

[10] Navon G, Eliav U, Demco D, Blümich B. Study of order and dynamic processes in tendon by NMR and MRI. Journal of Magnetic Resonance Imaging. 2007;25(2):362-380. doi:10.1002/jmri.20856

[11] Rössler E, Mattea C, Stapf S. Feasibility of high-resolution one-dimensional relaxation imaging at low magnetic field using a single-sided NMR scanner applied to articular cartilage. Journal of Magnetic Resonance. 2015;251:43-51. doi:10.1016/j.jmr.2014.10.014.

[12] Brizi L, Barbieri M, Baruffaldi F, et al. Bone volume-to-total volume ratio measured in trabecular bone by single-sided NMR devices. Magnetic Resonance in Medicine. 2017;79(1):501-510. doi:10.1002/mrm.26697

[13] Barbieri M, Brizi L, Bortolotti V, et al. Single-sided NMR for the diagnosis of osteoporosis: Diffusion weighted pulse sequences for the estimation of trabecular bone volume fraction in the presence of muscle tissue. Microporous and Mesoporous Materials. 2018;269:166-170. doi:10.1016/j.micromeso.2017.05.023.

[14] Rehorn C, Blümich B. Cultural Heritage Studies with Mobile NMR. Angewandte Chemie International Edition. 2018;57(25):7304-7312. doi:10.1002/anie.201713009.

[15] Wainwright SA, Marshall LM, Ensrud KE, et al. Hip Fracture in Women without Osteoporosis. J. Clin. Endocrinol. Metab. 2005;90:2787–2793.

[16] Granke M, Makowski AJ, Uppuganti S, Does MD, Nyman JS. Identifying Novel Clinical Surrogates to Assess Human Bone Fracture Toughness. Journal of Bone and Mineral Research. 2015;30(7):1290-1300. doi:10.1002/jbmr.2452.

[17] Blake GM, Fogelman I. The role of DXA bone density scans in the diagnosis and treatment of osteoporosis. Postgraduate Medical Journal. 2007;83(982):509-517. doi:10.1136/pgmj.2007.057505.

[18] Fantazzini P, Brown RJS, Borgia GC. Bone tissue and porous media: common features and differences studied by NMR relaxation. Magnetic Resonance Imaging. 2003;21(3-4):227-234. doi:10.1016/s0730-725x(03)00129-2.

[19] Fantazzini P, Bortolotti V, Brown RJS, et al. Two 1H-nuclear magnetic resonance methods to measure internal porosity of bone trabeculae: By solid–liquid signal separation and by longitudinal relaxation. Journal of Applied Physics. 2004;95(1):339-343. doi:10.1063/1.1630374

[20] Sigmund E, Cho H, Song Y-Q. High-resolution MRI of internal field diffusion-weighting in trabecular bone. NMR in Biomedicine. 2009;22(4):436-448. doi:10.1002/nbm.1354.

[21] Sprinkhuizen SM, Ackerman JL, Song Y-Q. Influence of bone marrow composition on measurements of trabecular microstructure using decay due to diffusion in the internal field MRI: Simulations and clinical studies. Magnetic Resonance in Medicine. 2013;72(6):1499-1508. doi:10.1002/mrm.25061.

[22] Mroue KH, Nishiyama Y, Pandey MK, et al. Proton-Detected Solid-State NMR Spectroscopy of Bone with Ultrafast Magic Angle Spinning. Scientific Reports. 2015;5(1). doi:10.1038/srep11991.

[23] Wehrli FW. Magnetic resonance of calcified tissues. Journal of Magnetic Resonance. 2013;229:35-48. doi:10.1016/j.jmr.2012.12.011.

[24] Wehrli FW, Song HK, Saha PK, Wright AC. Quantitative MRI for the assessment of bone structure and function. NMR in Biomedicine. 2006;19(7):731-764. doi:10.1002/nbm.1066.

[25] Tutunjian PN, Vinegar HJ, Edelstein WA. Automated core analysis by 1H NMR spectroscopy. Magnetic Resonance Imaging. 1991; 9 (5):859-864.

[26] Fernández-Seara M, Song H, Wehrli F. Trabecular bone volume fraction mapping by low-resolution MRI. Magnetic Resonance in Medicine. 2001;46(1):103-113. doi:10.1002/mrm.1165.

[27] Iita N, Handa S, Tomiha S, Kose K. Development of a compact MRI system for measuring the trabecular bone microstructure of the finger. Magnetic Resonance in Medicine. 2007;57(2):272-277. doi:10.1002/mrm.21130.

[28] Horch RA, Nyman JS, Gochberg DF, Dortch RD, Does MD. Characterization of 1H NMR signal in human cortical bone for magnetic resonance imaging. Magnetic Resonance in Medicine. 2010;64(3):680-687. doi:10.1002/mrm.22459.

[29] Seifert AC, Wehrli SL, Wehrli FW. Bi-component T2* analysis of bound and pore bone water fractions fails at high field strengths. NMR in Biomedicine. 2015;28(7):861-872. doi:10.1002/nbm.3305.

[30] Avioli LV. Significance of osteoporosis: A growing international health care problem. Calcified Tissue International. 1991;49(S1). doi:10.1007/bf02555078.

[31] Krug R, Burghardt AJ, Majumdar S, Link TM. High-Resolution Imaging Techniques for the Assessment of Osteoporosis. Radiologic Clinics of North America. 2010;48(3):601-621. doi:10.1016/j.rcl.2010.02.015.

[32] Hesse B, Langer M, Varga P, Pacureanu A, Pei Dong P, Schrof S, Maennicke N, Suhonen H, Olivier C, Maurer P, Kazakia GJ, RaumK, Peyrin F. Alterations of Mass Density and 3D Osteocyte Lacunar Properties in Bisphosphonate-Related Osteonecrotic Human Jaw Bone, a Synchrotron μCT Study. PLOS ONE. 2014;9(2):e88481.

[33] Giuliani A, Mazzoni S, Ruggiu A, Canciani B, Cancedda R, Tavella S. High-resolution X-ray tomography: a 3D exploration into the skeletal architecture in mouse models submitted to microgravity constraints. Frontiers in Physiology. 2018;9:181.

[34] Zebaze R, Atkinson EJ, Peng Y, Minh Bui M, Ghasem-Zadeh A, Khosla S, Seeman E. Increased Cortical Porosity and Reduced Trabecular Density Are Not Necessarily Synonymous With Bone Loss and Microstructural Deterioration, JBMR Plus. 2019;3(4):e10078. DOI: 10.1002/jbm4.10078,

[35] Parkinson IH, Badiei A, Fazzalari NL. Variation in segmentation of bone from micro-CT imaging: implications for quantitative morphometric analysis. Australasian Physics & Engineering Sciences in Medicine. 2008;31(2):160-164. doi:10.1007/bf03178592.

[36] Bortolotti V, Brown RJS, Fantazzini P. UpenWin: a software for inversion of multiexponential decay data for Windows system. Alma Mater Studiorum—Università di Bologna. 2012. (https://site.unibo.it/softwaredicam/en/software/upenwin) (Accessed: 29 March 2017)

[37] Bortolotti V, Brizi L, Fantazzini P, Landi G, Zama F. Filtering techniques for efficient inversion of two-dimensional Nuclear Magnetic Resonance data. Journal of Physics: Conference Series. 2017;904:012005. doi:10.1088/1742-6596/904/1/012005.

[38] Borgia G, Brown R, Fantazzini P. Uniform-Penalty Inversion of Multiexponential Decay Data. Journal of Magnetic Resonance. 1998;132(1):65-77. doi:10.1006/jmre.1998.1387.

[39] Borgia G, Brown R, Fantazzini P. Uniform-Penalty Inversion of Multiexponential Decay Data: II data spacing, T2 data, systematic data errors, and diagnostics. Journal of Magnetic Resonance. 2000;147(2):273-285. doi:10.1006/jmre.2000.2197.

[40] Granke M, Does MD, Nyman JS. The Role of Water Compartments in the Material Properties of Cortical Bone. Calcified Tissue International. 2015;97(3):292-307. doi:10.1007/s00223-015-9977-5.

[41] Horch RA, Gochberg DF, Nyman JS, Does MD. Non-invasive Predictors of Human Cortical Bone Mechanical Properties: T2-Discriminated 1H NMR Compared with High Resolution X-ray. PLoS ONE. 2011;6(1). doi:10.1371/journal.pone.0016359.

[42] Stephen C. Cowin. Bone poroelasticity, Journal of Biomechanics, 32 (1999) 217-238.

[43] Seeman E, Delmas PD. Bone quality – the material and structural basis of bone strength and fragility. N Engl J Med. 2006; 354:2250–2261.

[44] Chen J, Grogan SP, Shao H, D'Lima D, Bydder GM, Wu1 Z, Du J. Evaluation of Bound and Pore Water in Cortical Bone Using Ultrashort Echo Time (UTE) Magnetic Resonance Imaging, NMR Biomed. 2015 December; 28(12): 1754–1762. doi:10.1002/nbm.3436.

[45] Biswas R, Bae W, Diaz E, et al. Ultrashort echo time (UTE) imaging with bi-component analysis: Bound and free water evaluation of bovine cortical bone subject to sequential drying. Bone. 2012;50(3):749-755. doi:10.1016/j.bone.2011.11.029.

List of Figure

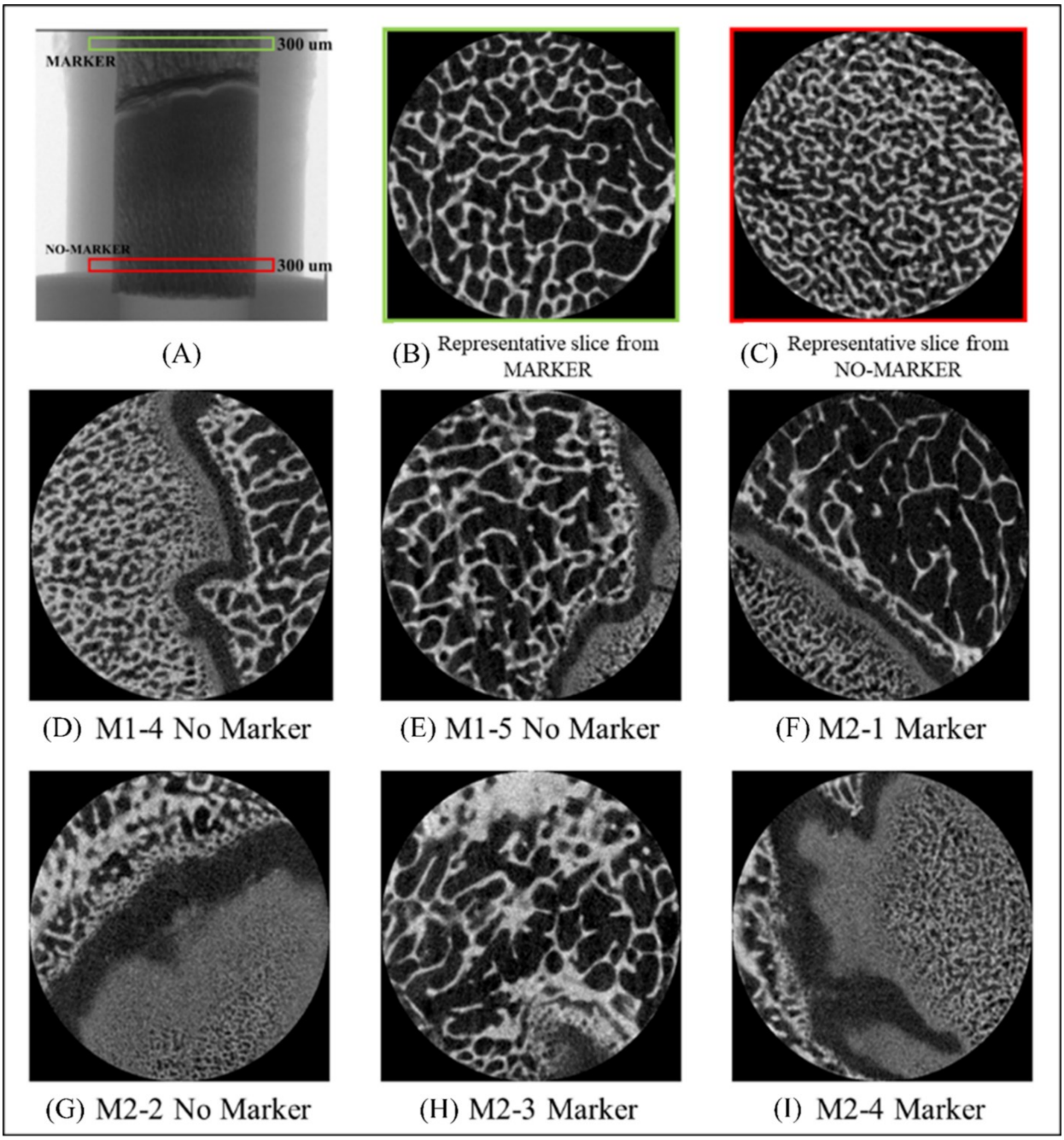

Figure 1. Examples of micro-CT analysis of trabecular bones. (A) coronal view of a micro-CT scan, with the positions of the two sensitive volumes chosen for the NMR acquisitions, (B) and (C) axial micro-CT images acquired on the two corresponding ROIs for a sample where only bone and bone marrow were present. The sensitive volume (300 µm thick) was located at 3 mm from the coil surface. Although ROIs selection was performed with care, it is possible that the positions of the slices chosen for the micro-CT analysis could differ on the order of a few tens of microns from those intercepted by the NMR sensitive volume. From (D) to (I), slice examples are provided from micro-CT images of the 6 more heterogeneous samples containing growth cartilage, which has the same gray level as marrow, and less mineralized bone tissue, that appears less intense than bone in the images. “M2-2 No Marker” and “M2-4 Marker” (G) and (I) are the two samples excluded from the analysis (see Results).

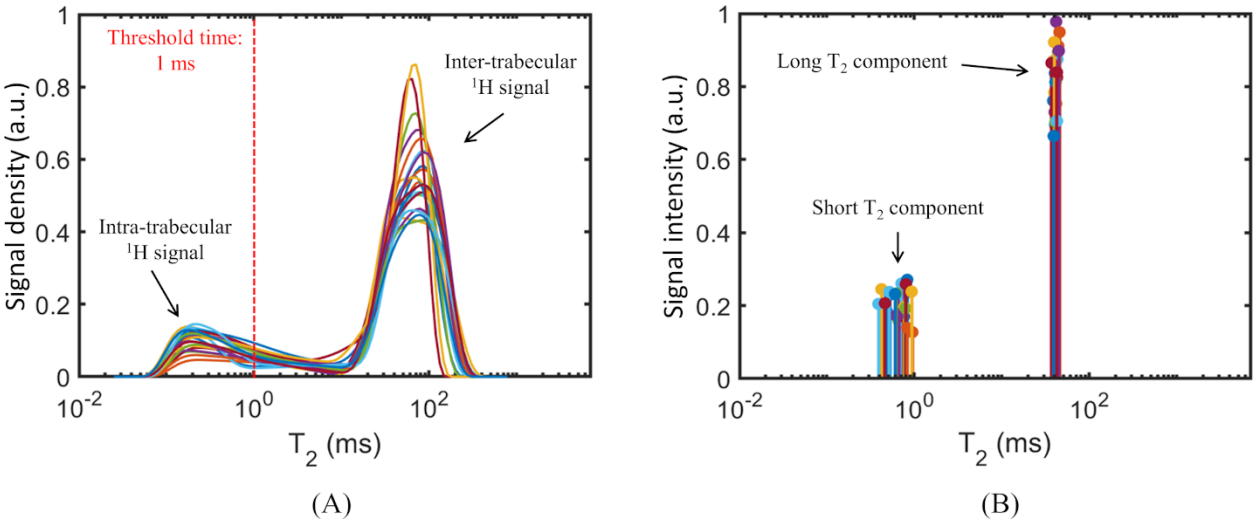

Figure 2. T_2 distributions of all the trabecular bone samples examined. (A) quasi-continuous T_2 distributions computed with the algorithm UPEN, (B) bi-component distributions evaluated with bi-exponential fits of the same experimental CPMG data. In (A), the threshold time, set at 1 ms, used to distinguish the intra- from the inter-trabecular ^{1}H signals is displayed as a dashed red vertical line.

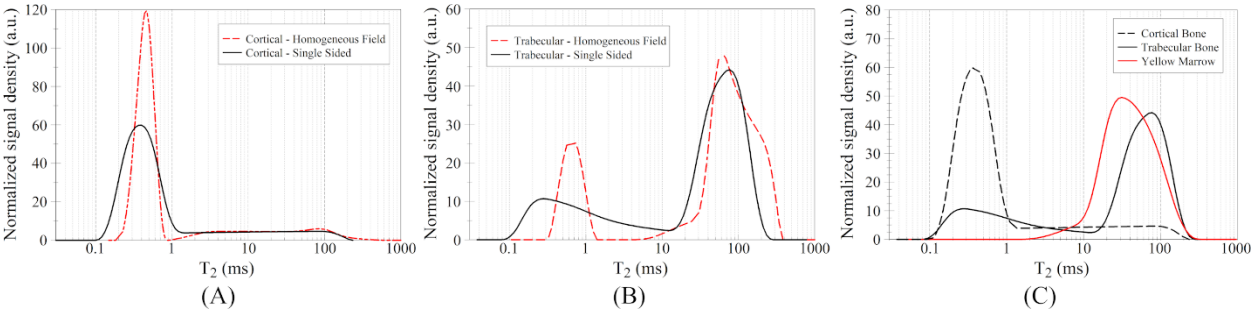

Figure 3. T_2 quasi-continuous distributions of cortical bone, trabecular bone and bulk marrow obtained by CPMG data acquired by a home-made relaxometer characterized by a homogeneous magnetic field B_0 = 0.47 T, and by the NMR MOUSE PM10. (A) Cortical bone by both instruments, (B) trabecular bone by both instruments, (C) cortical bone, trabecular bone and bulk marrow by MOUSE PM10. Comparison of the distributions supports the use of a 1 ms threshold to distinguish the signals from intra- and inter-trabecular compartments in the trabecular bone.

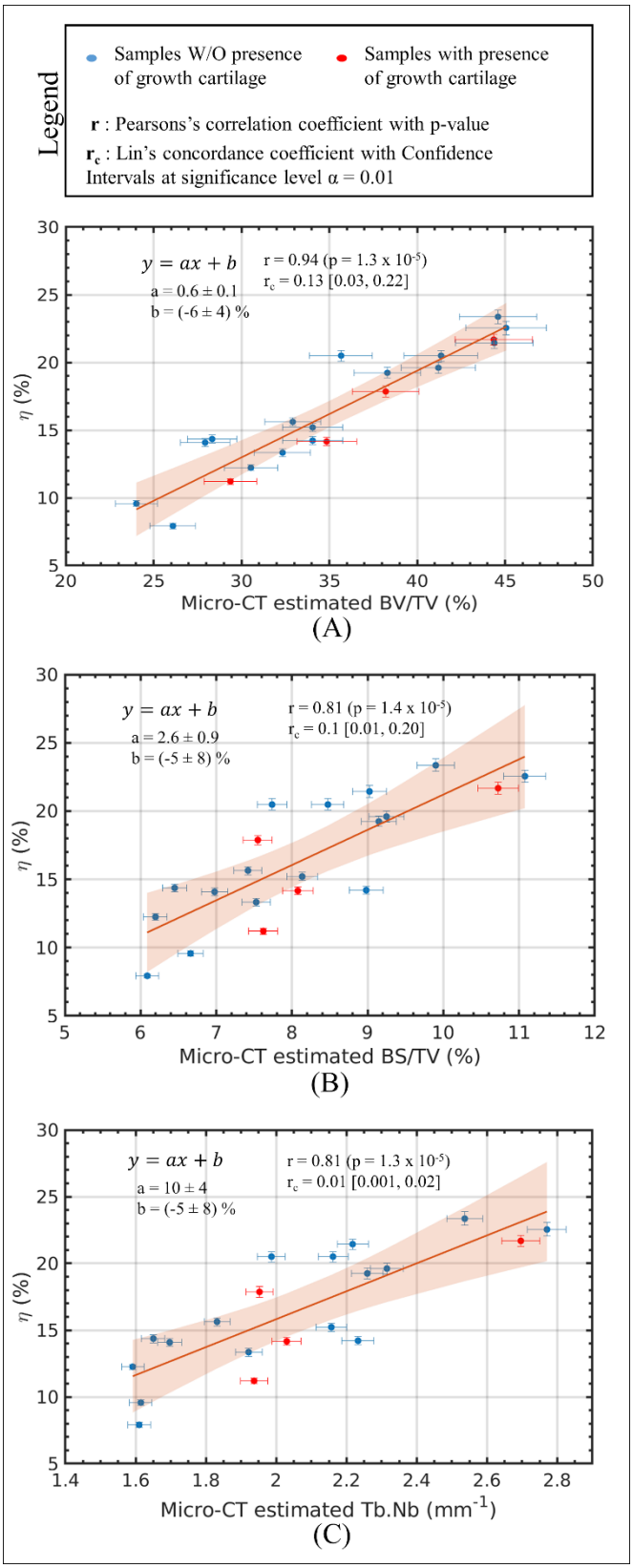

Figure 4. (A, B, C) Plots of η, the short T_2 intensity fraction, evaluated using the quasi-continuous T_2 distributions, against the morphological parameters evaluated by the micro-CT analyses. (A) *BV/TV*, (B) *BS/TV*, (C) *Tb.Nb*. The four samples that, based on micro-CT images, presented growth cartilage are marked with red dots in the plots. Significance levels for *BV/TV*, *BS/TV*, and *Tb.Nb* were $p = 1.3\times10^{-9}$, 1.4×10^{-5}, and 1.3×10^{-5}, respectively.

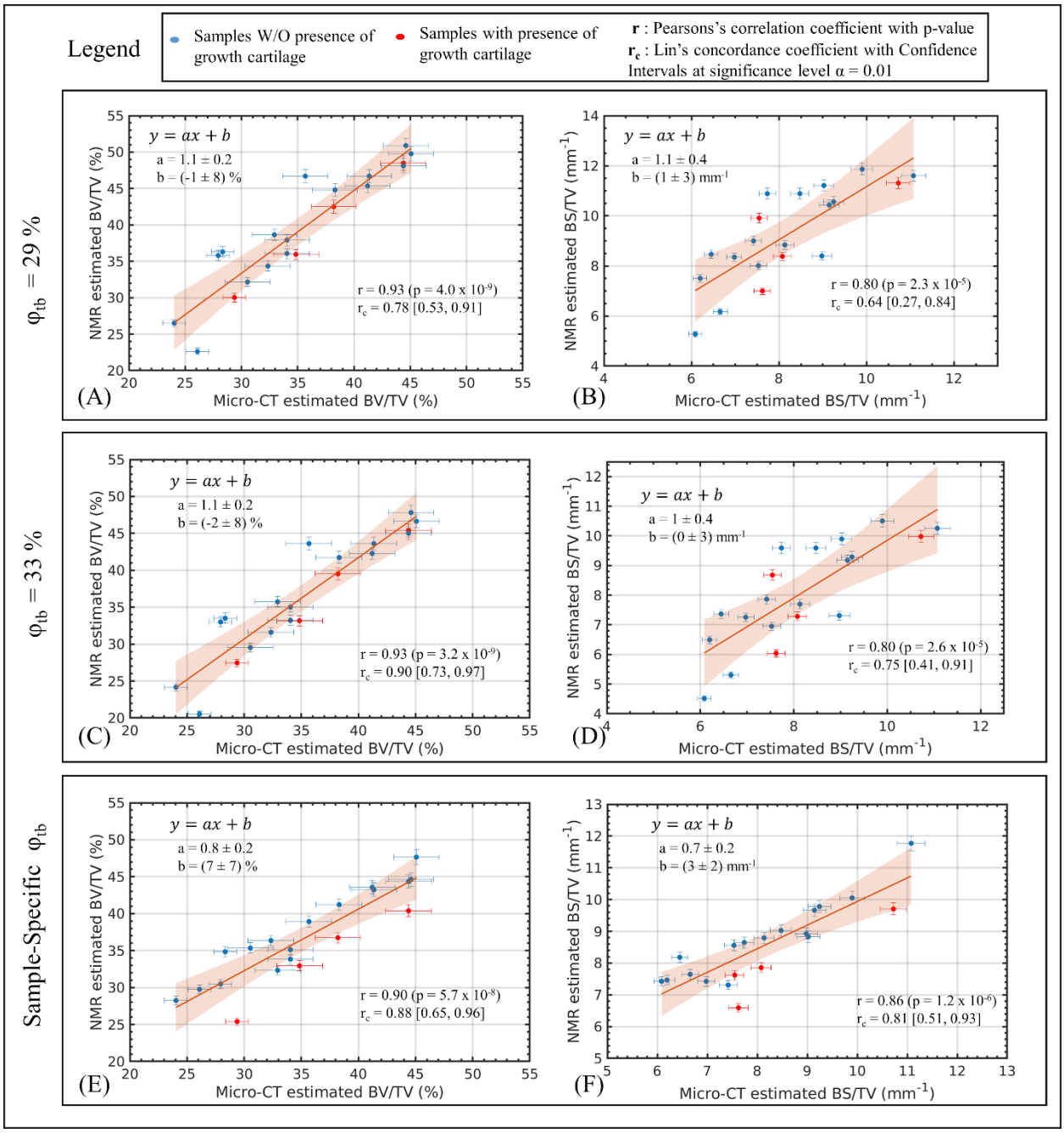

Figure 5. Comparison between NMR and micro-CT estimated morphological parameters. In (A), (C) and (E) *BV/TV*; in (B), (D) and (F) *BS/TV*. The NMR parameter were estimated in (A) and (B) using φ_{tb} =29%; in (C) and (D) φ_{tb} =33%; in (E) and (F) the individual sample specific φ_{tb}, as reported in Table 3 for each sample, was used, requiring the use of a reference signal. For the NMR estimation of *BS/TV* we used R = 86 μm. The linear fits have slopes close to 1 and bias terms close to zero. The Pearson's and Lin's coefficients were reported. It is worth noting (Figure 5E and 5F) that the use of the individual sample specific value for φ_{tb} moved the four samples with cartilage (red dots) below the best fit line.

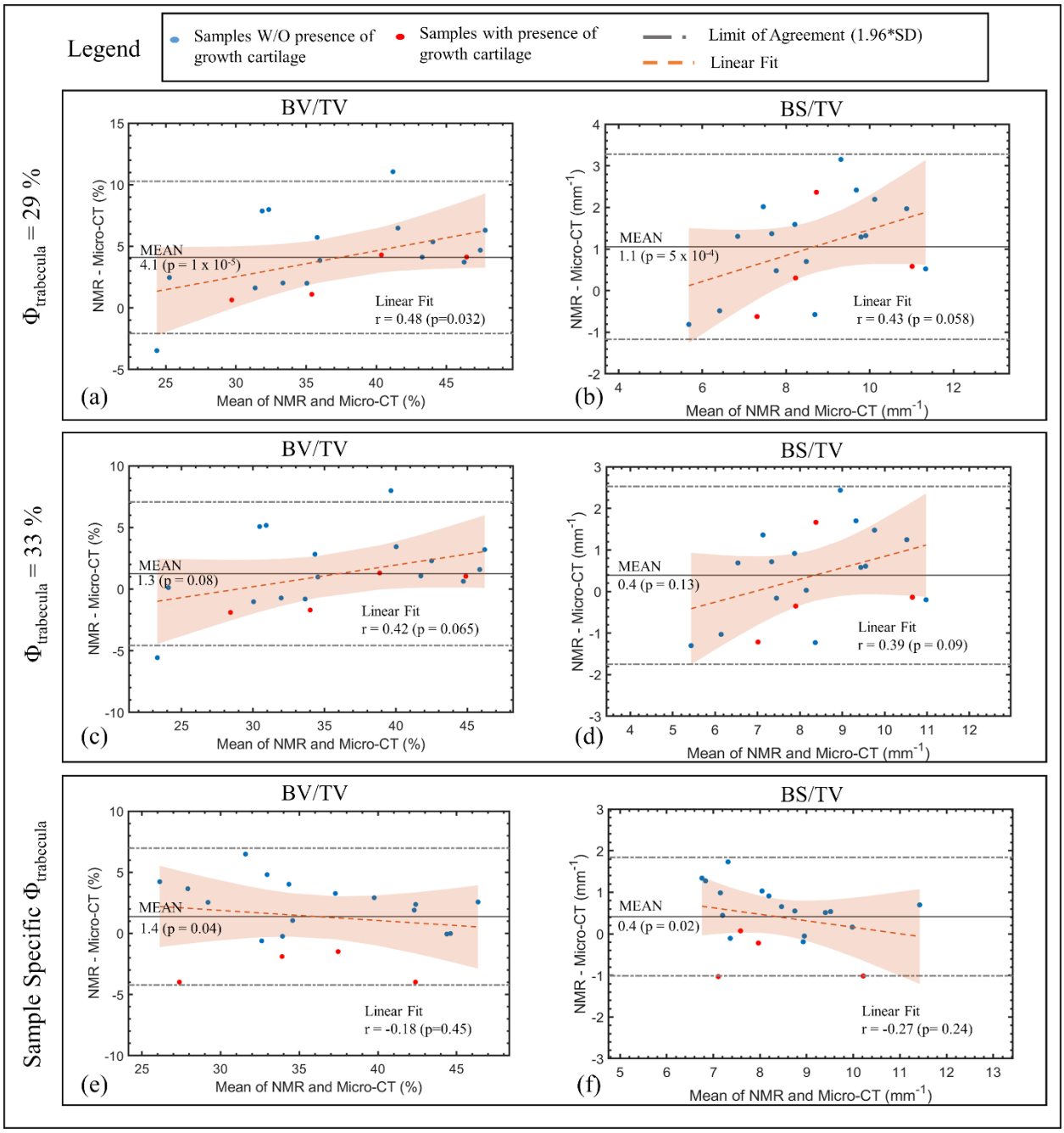

Figure 6. Bland-Altman (B-A) plots for the comparison of NMR and micro-CT estimates of morphological parameters *BV/TV* and *BS/TV* are reported. For each B-A plot, the following statistics are reported: i) the mean value of the differences (i.e. mean bias, horizontal solid line), reported along with the p-value of the t-test where the null hypothesis is that the differences come from a normal distribution with mean equal to zero and unknown variance; ii) the limits of agreement (horizontal dashed-dotted lines) and iii) the linear regression fit (red dashed line) along with correlation coefficient and corresponding p-value. The NMR estimates were evaluated using different values for φ_{tb}. In Figure 6A and 6B, the mean value of the trabecular porosity available in literature [19] (φ_{tb} = 29%) was used. In Figure 6C and 6D the mean value of our samples, φ_{tb} =33% (Table 3) was used. In Figure 6E and 6F, the individual φ_{tb} estimated for each sample was used, a procedure that requires the reference signal.

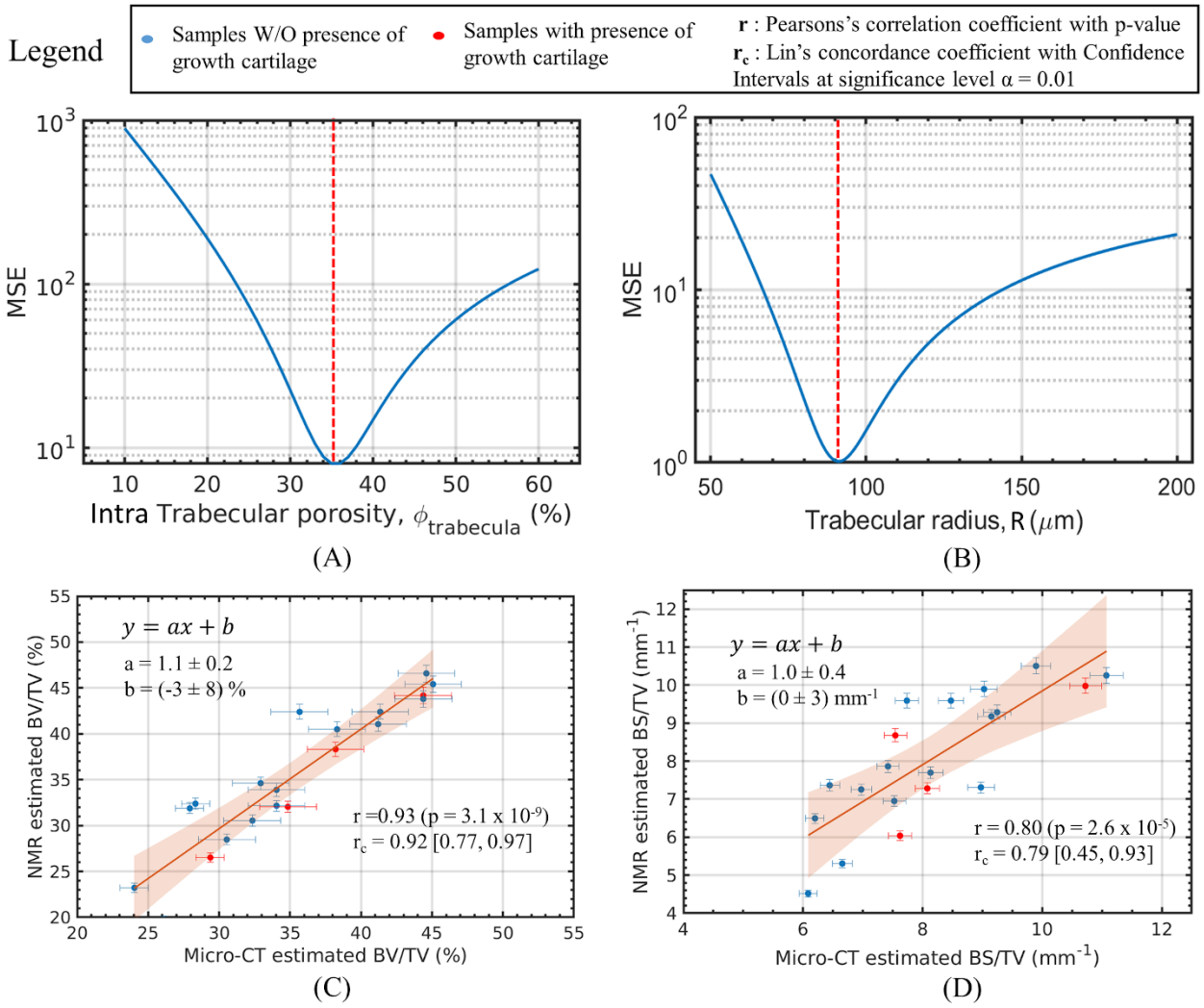

Figure 7. Minimization of the error of the fit between NMR and micro-CT parameters. (A) Mean Squared Error (MSE) between NMR and micro-CT estimated *BV/TV* as a function of the φ_{tb} parameter used in Eq. 5. (B) MSE between NMR and micro-CT estimated *BS/TV* as a function of the trabecular radius, *R* used in Eq.7. The best value of φ_{tb} to minimize the error on the estimation of *BV/TV* was found to be 35% (Figure 7A) and to minimize the error on *BS/TV* was found to be 90 μm (Figure 7B). In (C) and (D) the plots are reported of the NMR against micro-CT estimates of the two parameters, computed with the minimization values found in (A) and (B), respectively. Linear model coefficients (Figure 7C and 7D) do not significantly differ from those reported in Figure 5C and 5D. The value 35% belong to the interval (33±5) % in Table 3, and 90 μm is consistent with half the sample mean trabecular thickness (Table 2).